

Article

# Structural Bases for the Fitness Cost of the Antibiotic-Resistance and Lethal Mutations at Position 1408 of 16S rRNA

Jiro Kondo \*  and Mai Koganei

Department of Materials and Life Sciences, Faculty of Science and Technology, Sophia University, 7-1 Kioi-cho, Chiyoda-ku, Tokyo 102-8554, Japan

\* Correspondence: j.kondo@sophia.ac.jp

Academic Editor: Quentin Vicens

Received: 4 October 2019; Accepted: 29 December 2019; Published: 31 December 2019



**Abstract:** To understand a structural basis for the fitness cost of the A1408G antibiotic-resistance mutation in the ribosomal A-site RNA, we have determined crystal structures of its A1408C and A1408U lethal mutants, and made comparison with previously solved structures of the wild type and the antibiotic-resistant mutant. The A-site RNA containing an asymmetric internal loop functions as a molecular switch to discriminate a single cognate tRNA from several near-cognate tRNAs by its conformational ON/OFF switching. Overall structures of the “off” states of the A1408C/U lethal mutants are very similar to those of the wild type and the A1408G antibiotic-resistant mutant. However, significant differences are found in local base stacking interactions including the functionally important A1492 and A1493 residues. In the wild type and the A1408G antibiotic-resistant mutant “off” states, both adenines are exposed to the solvent region. On the other hand, one of the corresponding adenines of the lethal A1408C/U mutants stay deeply inside their A-site helices by forming a purine-pyrimidine AoC or A-U base pair and is sandwiched between the upper and lower bases. Therefore, the ON/OFF switching might unfavorably occur in the lethal mutants compared to the wild type and the A1408G antibiotic-resistant mutant. It is probable that bacteria manage to acquire antibiotic resistance without losing the function of the A-site molecular switch by mutating the position 1408 only from A to G, but not to pyrimidine base C or U.

**Keywords:** antibiotic resistance; fitness cost; decoding; molecular switch; ribosome

## 1. Introduction

The aminoacyl-tRNA decoding site (A site) is one of the active sites of the ribosome where a single cognate tRNA is accurately discriminated from several near-cognate tRNAs [1–4]. In the decoding process, an RNA internal loop (Figure 1) composed of fifteen nucleotide residues functions as a molecular switch by changing its conformation between “off” and “on” states. Crystallographic studies of several ribosomal particles [5–22] as well as RNA fragments containing the A-site molecular switches [23–30] have revealed the molecular mechanism of the decoding process at atomic level, especially in the case of bacteria. Two consecutive adenines A1492 and A1493 in the asymmetric internal loop are the most important residues for the function of the molecular switch. In the absence of aminoacyl-tRNA, these two adenines can take various conformations, which are called as “off” states where both of or one of two adenines stay inside the A-site helix and form a base pair with the 1408 residue on the opposite strand. Once an aminoacyl-tRNA is delivered to and occupies the A site, the RNA molecular switch changes its conformation to a unique “on” state, in which two adenines A1492 and A1493 fully bulge out from the A-site helix, protrude toward the mRNA-tRNA complex and recognize the first two base pairs of the codon-anticodon mini-helix through A-minor motifs to

check their geometries. If these base pairs are of the canonical Watson–Crick type, the aminoacyl-tRNA is recognized as the cognate one and can be accommodated by the ribosome. These two functional adenine residues are universally conserved as expected from their biological significances [31]. On the other hand, the 1408 residue on the opposite strand of the A-site internal loop must be a purine, but varies across the different organisms and organelles. For example, it is adenine in prokaryotes, mitochondria and chloroplasts, and is mostly guanine in eukaryotic cytoplasm [31].

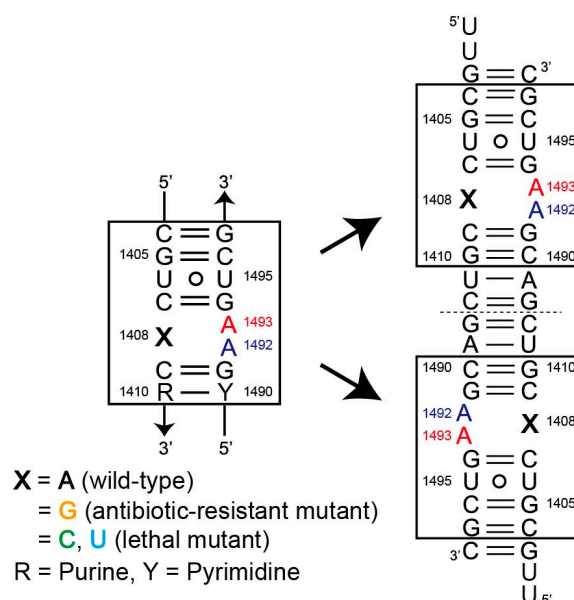


**Figure 1.** Secondary structures of the RNA duplexes used in our present and previous crystallographic studies. The two bacterial A-site molecular switches are boxed. A uracil residue at position 11 is replaced by a 5-bromouracil in bromine-derivatives. Two adenine residues A1492 and A1493 that recognize the codon-anticodon helix are colored in blue and red, respectively.

A single chromosomal mutation at position 1408 of the bacterial 16S rRNA from A to G is the most prevalent antibiotic-resistant mutation found in clinical isolates [32–41]. The A1408G mutation confers high-level resistance against aminoglycosides with an ammonium group at position 6′ on ring I [42–47], and its structural basis has recently been revealed by our X-ray analyses; ring I with 6′-NH<sub>3</sub><sup>+</sup> can make a pseudo pair with A1408 of the wild type but cannot make the identical pseudo pair with G1408 of the antibiotic-resistant mutant due to repulsive force between 6′-NH<sub>3</sub><sup>+</sup> of ring I and N1-H and N2-H of G1408 [29]. In general, the antibiotic resistance is strongly associated with the fitness cost, which is observed as a reduced growth rate in the absence of antibiotics [48]. However, it was confirmed by Böttger and coworkers that the generation time is almost the same for the wild type (2.98 ± 0.06 h) and the A1408G antibiotic-resistant mutant (3.15 ± 0.06 h) strains of *Mycobacterium smegmatis* grown in broth culture [49], indicating that the A1408G antibiotic-resistant mutation does not affect the fitness of bacteria so much [49,50]. In our previous X-ray analyses, we have confirmed that the structures of the “off” and “on” states of the A1408G antibiotic-resistant mutant A site are very similar to those of the wild type A site. Therefore, it would appear that the A1408G antibiotic-resistant mutation does not disturb the function of the A-site molecular switch [29]. Now, an important question arises; why must the 1408 residue be a purine? Neither prokaryotic nor eukaryotic organisms have a pyrimidine at the position [31]. In fact, the A1408C and A1408U mutations are lethal to bacteria [49]. Another mutation experiment revealed that A1408U mutation significantly decreases protein expression [51]. Herein, we have performed X-ray analyses of RNA fragments containing the lethal-mutant A sites to see whether these mutations disturb the function of the RNA molecular switch.

## 2. Results and Discussion

### 2.1. Structures of the A1408C Lethal Mutant A Site and Its Comparison with the Wild Type and the A1408G Antibiotic-Resistant Mutant

For the A1408C lethal mutant A site, two types of crystals, A1408C-Br/geneticin and A1408C-Br, were obtained in the presence and absence of aminoglycoside geneticin, respectively (Figure 2). In each crystal, one RNA duplex is in the asymmetric unit, meaning that a total of four A-site switches are observed. In the absence of aminoglycoside, two A-site molecular switches take different “off” conformations (Figure 2b), one with bulged-in A1492 and A1493 (the “off” state form 1, hereafter; Figure 3a) and one with bulged-out A1492 and bulged-in A1493 (the “off” state form 2, hereafter; Figure 4a). In the presence of geneticin, the two A-site molecular switches are stabilized in the “on” state conformation with bulged-out adenines A1492 and A1493 (Figures 2b and 5a).

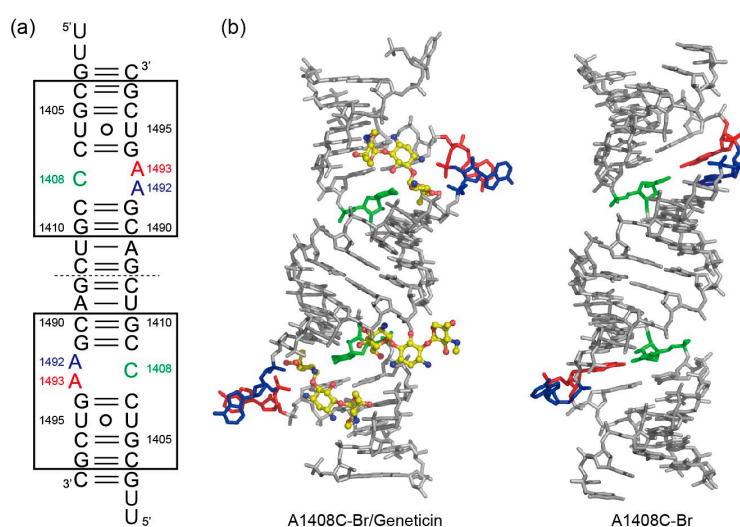


**Figure 2.** (a) Secondary structures of the RNA duplexes containing two A1408C mutant A-site molecular switches used in the crystallographic studies. (b) Tertiary structures of the RNA duplexes in the asymmetric unit of the A1408C-Br/geneticin and A1408C-Br crystals.

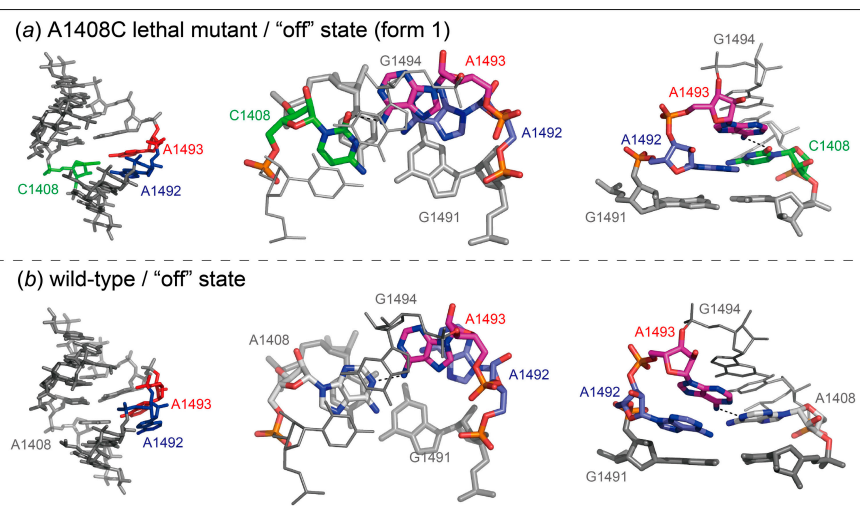


**Figure 3.** Molecular structures (left) and close-up views of base pairs (center) and stacking interactions (right) observed in the “off” state form 1 of the bacterial A1408C lethal mutant (a) and wild type (28: PDB-ID = 3BNL) (b) A sites.

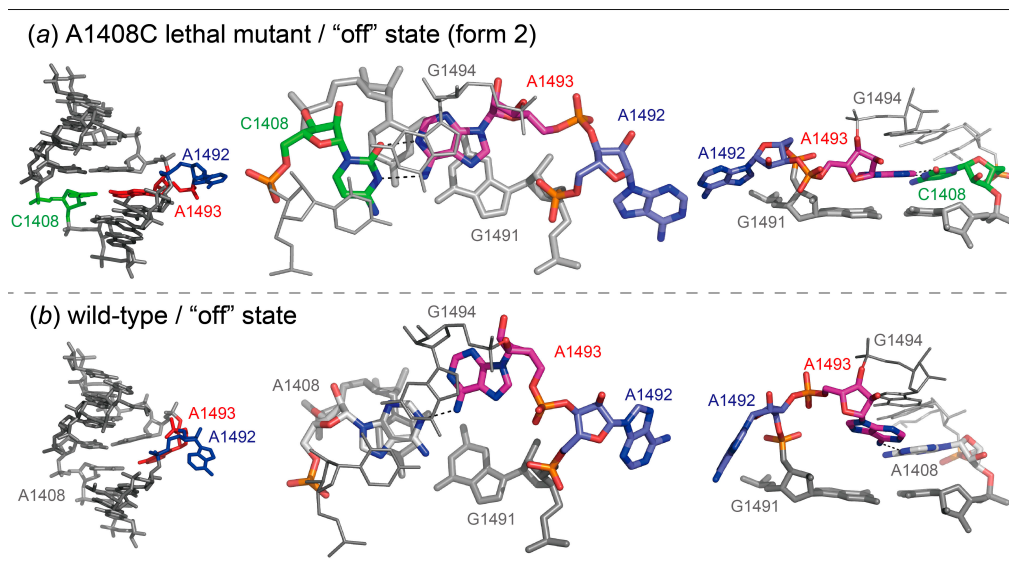


**Figure 4.** Molecular structures (left) and close-up views of base pairs (center) and stacking interactions (right) observed in the "off" state form 2 of the bacterial A1408C lethal mutant (a) and wild type (28: PDB-ID = 3BNL) (b) A sites.

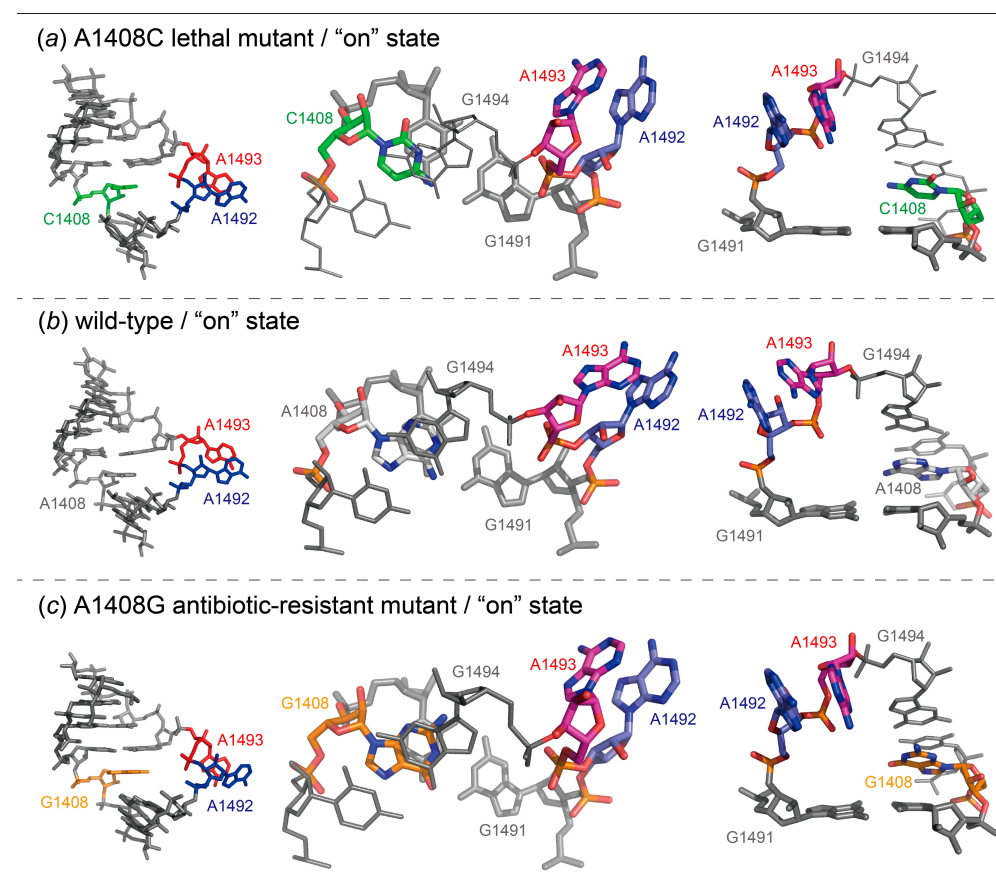


**Figure 5.** Molecular structures (left) and close-up views of base pairs (center) and stacking interactions (right) observed in the "on" state of the bacterial A1408C lethal mutant (a), wild type (12: PDB-ID = 2J00) (b) and the A1408G antibiotic-resistant mutant (29: PDB-ID = 3TD1) (c) A sites. For better understanding, geneticin and paromomycin bound to these A sites are removed.

In the “off” state form 1 (Figure 3a), the bulged-in A1493 forms a base pair with C1408 and stacks below G1494. The other bulged-in adenine A1492 does not make base pair in the A-site helix but stacks between A1493 and G1491. As a result, a stacking column G1494-A1493-A1492-G1491 is observed in the A-site helix. The “off” state form 1 is similar to the wild type “off” state with bulged-in A1492 and A1493 determined by our group (Figure 3 and Figure S1) [28]. In both cases, the bulged-in A1493 residue forms a base pair with the C/A1408 residue through only one hydrogen bond,  $N6_{A1493}-H\dots O2_{C1408}$  or  $N6_{A1493}-H\dots N1_{A1408}$ . The C1'-C1' distances are 10.8 Å for the AoC base pair and 12.5 Å for the AoA base pair, respectively. Therefore, the A1493 residue is inserted more deeply into the A-site helix in the A1408C lethal mutant than in the wild type. Difference is found also in the conformation of the other bulged-in adenine. In the A1408C lethal mutant, A1492 is deeply inserted into the A-site helix and sandwiched between A1493 and G1491, and is thereby involved in a long stacking column from G1497 to C1490. In the wild type, however, the corresponding adenine residue A1492 is not inserted into the A-site helix, just stacks under A1493 and is partly exposed to the solvent region at the other side, so that two stacking columns from G1497 to A1492 and from G1491 to C1490 are formed. The distance between C1' atoms of A1492 and C/A1408 are 12.5 and 14.5 Å, respectively. In consequence, the ribose rings of the A1492 and A1493 residues, which are fitted into the regular A-form helix in the A1408C lethal mutant “off” state form 1, are partly protruded from the A-site helix in the wild type “off” state.

In the “off” state form 2 (Figure 4a), the bulged-in A1493 forms a base pair with C1408. Since the neighboring A1492 residue fully bulges out from the A-site helix, the A1493 residue is intercalated between G1494 and G1491. The “off” state form 2 is similar to the wild type “off” state with bulged-out A1492 and bulged-in A1493 solved by our group (Figure 4 and Figure S2) [28]. In both A sites, A1492 bulges out from the A-site helix toward the solvent region where aminoacyl-tRNAs are delivered. In the A1408C lethal mutant, the bulged-in A1493 residue forms a base pair with C1408 through two hydrogen bonds  $N6_{A1493}-H\dots N3_{C1408}$  and  $N1_{A1493}-H\dots O2_{C1408}$ . For making the base pair, the N1 atom of A1493 has to be protonated. In fact, the A<sup>+</sup>oC base pair is often observed in the 16S and 23S ribosomal RNAs [52,53], where RNA strands with acidic phosphate groups are compactly folded and packed. The C1'-C1' distance of the A<sup>+</sup>oC base pair is 10.1 Å, which is slightly shorter than that of the canonical Watson–Crick base pairs (10.7 Å in average) [54]. The corresponding residue A1493 in the wild type “off” state forms a pair with A1408 through  $N6_{A1493}-H\dots N1_{A1408}$  with the C1'-C1' distance of 12.5 Å. Since A1493 of the A1408C lethal mutant is inserted more deeply into the A-site helix, the residue is intercalated between G1494 and G1491 and involved in a long stacking column. On the other hand, the A1493 residue of the wild type stacks only with G1494 and is partly exposed to the solvent region at the other side.

The “on” state of the A1408C lethal mutant is identical to that of the wild type as observed, for example, in the 70S ribosome structure solved by Ramakrishnan and coworkers [12], and also to that of the A1408G antibiotic-resistant mutant solved by our group [29] (Figure 5 and Figure S3). In the “on” state, both A1492 and A1493 largely bulge out from the A-site helix to recognize the mRNA-tRNA mini-helix, but make no intra-molecular interactions.

These observations suggest that the “off” state conformations are strongly correlated with the fact that the A1408C mutation is lethal to bacteria. The wild type A-site molecular switch can easily change its conformation from the “off” to “on” states, since the A1492 and A1493 residues essential for the decoding are partly exposed to the solvent region even in the “off” states. On the other hand, the corresponding adenine residues of the A1408C lethal mutant are stabilized in the long base-stacking column, and the ON/OFF switching might unfavorably occur in the lethal mutant compared to the wild type.

## 2.2. Structures of the A1408U Lethal Mutant A Site and Its Comparison with the Wild Type and the A1408G Antibiotic-Resistant Mutant

For the A1408U lethal mutant A site, two different crystals, A1408U/geneticin and A1408U-Br, were obtained in the presence and absence of geneticin, respectively (Figure 6). In the A1408U/geneticin crystal, one RNA duplex is observed in the asymmetric unit, but electron density of geneticin is not observed. In the A1408U-Br crystal, two RNA duplexes are in the asymmetric unit. Therefore, a total of six A-site molecular switches are obtained from the two crystals. Interestingly, all these six A-site internal loops take an identical “off” state conformation with bulged-in A1492 and bulged-out A1493 (Figure 7a and Figure S4). The “off” state is similar to the wild type “off” state with bulged-in A1492 and bulged-out A1493 as solved by Hermann and coworkers [24] (Figure 7 and Figure S5). In addition, the “off” state is also similar to the A1408G antibiotic-resistant mutant “off” state determined by our group (Figure 7 and Figure S5) [29]. In these A sites, A1493 fully bulges out from the A-site helix and points toward the solvent region where aminoacyl-tRNAs are delivered. In the A1408U lethal mutant, the bulged-in A1492 residue forms a canonical Watson–Crick A-U base pair with U1408. The C1′-C1′ distance of the base pair is 11.1 Å. The corresponding residue A1492 in the wild type “off” state forms a pair with A1408 through N1<sub>A1492</sub>...H-N6<sub>A1408</sub> with the C1′-C1′ distance of 12.3 Å. In the A1408G antibiotic-resistant mutant “off” state, a *cis* Watson–Crick A1492oG1408 base pair is formed through two hydrogen bonds N6<sub>A1492</sub>-H...O6<sub>G1408</sub> and N1<sub>A1492</sub>...H-N1<sub>G1408</sub> with the C1′-C1′ distance of 12.7 Å. Since the A1492 residue of the A1408U lethal mutant forms the canonical Watson–Crick A-U base pair, the residue is well fitted into the regular A-form helix and intercalated between G1494 and G1491. On the other hand, the corresponding residues of the wild type and the A1408G antibiotic-resistant mutant A sites stack only on G1491 and expose their base moieties to the solvent region at the other side.

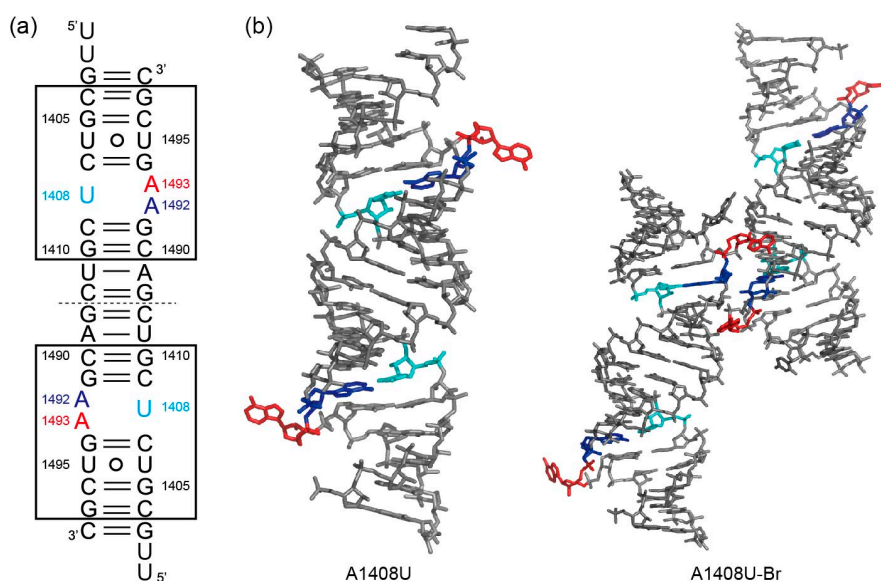


**Figure 6.** (a) Secondary structures of the RNA duplexes containing two A1408U mutant A-site molecular switches used in the crystallographic studies. (b) Tertiary structures of the RNA duplexes in the asymmetric unit of the A1408U/geneticin and A1408U-Br crystals.

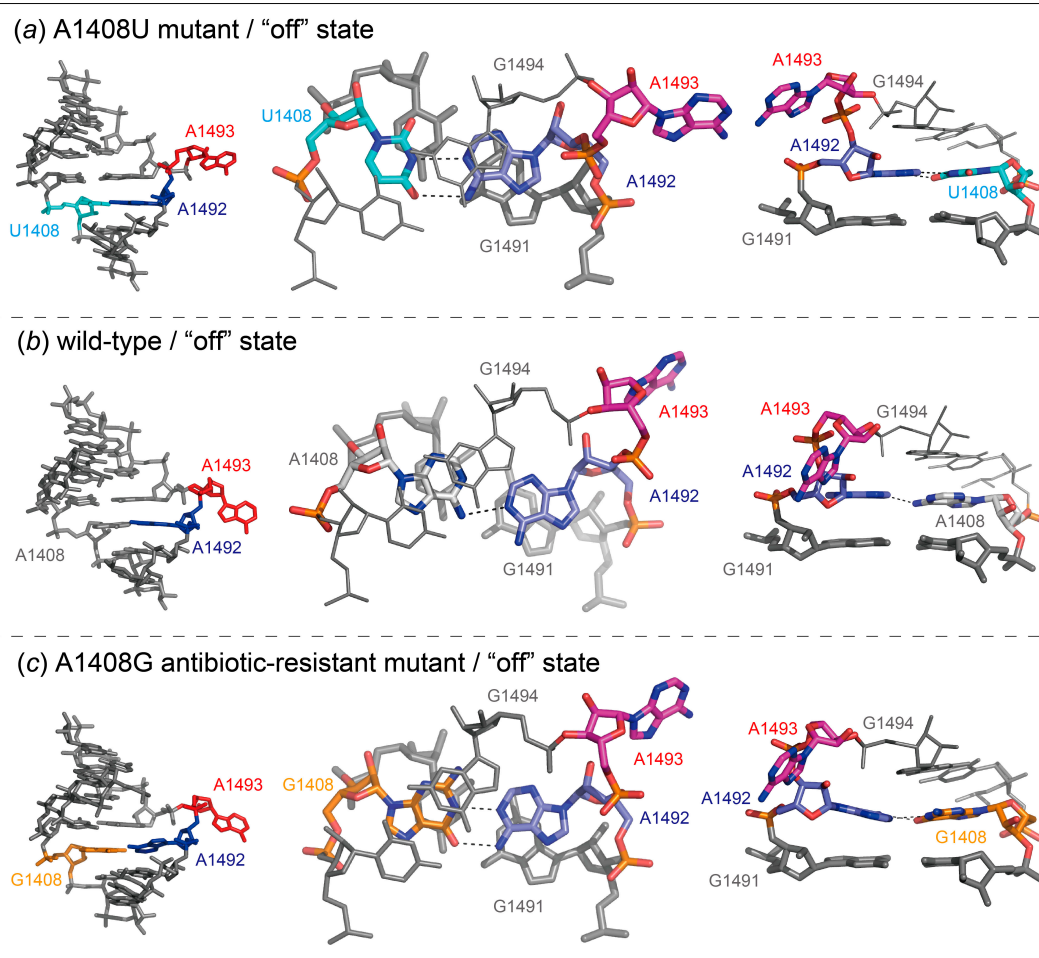


**Figure 7.** Molecular structures (left) and close-up views of base pairs (center) and stacking interactions (right) observed in the "off" state of the bacterial A1408U lethal mutant (a), wild type (24: PDB-ID = 1T0E) (b) and the A1408G antibiotic-resistant mutant (29: PDB-ID: 3TD0) (c) A sites.

From these observations, it would appear that the bulged-in A1492 residue of the wild type and the A1408G antibiotic-resistant mutant RNA molecular switches is likely to bulge out when the aminoacyl-tRNA is delivered to the A site. It is consistent with the fact that the generation time is almost the same for the wild type and the A1408G antibiotic-resistant mutant strains of *M. smegmatis* grown in broth culture [49]. However, the A1408U lethal mutant A site prefers to take a single stable "off" state where the A1492 residue is comfortably fitted into the A-site helix by forming the canonical Watson–Crick base pair with U1408 and stacking interactions with G1494 and G1491. It can be expected from the structural comparison that the ON/OFF switching of the A1408U lethal mutant A site might be energetically unfavorable compared to that of the wild type and the A1408G antibiotic-resistant mutant A sites.

### 2.3. Conclusions of Discussion

Bulges and internal loops are the most popular structural motifs observed in RNA molecules. However, little is known about their sequence-dependent structural and dynamic features. The ribosomal A-site internal loop composed of fifteen nucleotides including three highly-conserved residues, A/G1408, A1492 and A1493, has a characteristic feature that dynamically changes its conformation between the "off" (A1492 and/or A1493 are bulged in) and "on" (both A1492 and A1493 are fully bulged out) states, and functions as a molecular switch for discriminating a single cognate tRNA from several near-cognate tRNAs. In our previous studies [25,28,29], we have shown how

small differences of nucleotide sequences affect the dynamics of the A-site molecular switches. Herein, we have further shown why the 1408 residue must be universally a purine. The 1408 residue strongly affects not only the base pair formation but also the stacking manner of A1492 and A1493 on the opposite strand. In the “off” state of the wild type and the A1408G antibiotic-resistant mutant A sites, the bulged-in A1492 or A1493 residue forming a base pair with A/G1408 are partly exposed to and are ready to bulge out toward the mRNA-tRNA helix for taking the “on” state. If the 1408 residue is a pyrimidine as observed in the A1408C/U lethal mutants, the A-site internal loop may lose its function as a molecular switch by taking the energetically stable “off” state where bulged-in A1492 or A1493 stays deeply inside the A-site helix by forming the purine-pyrimidine base pair, AoC or A-U. It is also important to note that the stability of the base pair between the residue at position 1408 and A1492/A1493 residues is not a critical factor, since the number of hydrogen bonds observed in the base pair is one or two in any case. It is probable that all organisms naturally select a purine at the position 1408, and bacteria can acquire antibiotic resistance without losing the function of the A-site molecular switch by mutating position 1408 from A to G, but not to pyrimidine base C or U.

### 3. Materials and Methods

#### 3.1. Sample Preparations and Crystallizations

RNA duplexes containing two bacterial A-site molecular switches with a single A1408C or A1408U lethal point mutation were designed for the present crystallographic studies (Figure 1). Such RNA fragments have been extensively used as successful models in a series of crystallographic studies [23–29], since their crystal packing mimic highly-crowded environment of the A site in the ribosome. These RNA oligomers (A1408C and A1408U, hereafter), and their bromine derivatives for phase determinations (A1408C-Br and A1408U-Br, hereafter), were chemically synthesized by Dharmacon (Boulder, CO, USA) and GeneDesign (Osaka, Japan), and then purified by denaturing 20% polyacrylamide gel electrophoresis and C18 reversed-phase chromatography.

Crystallizations were performed in both the absence and presence of aminoglycoside geneticin (also known as G418). By analogy with our previous crystallographic studies of the bacterial wild type and the A1408G antibiotic-resistant mutant A sites [28,29], it can be expected that the lethal mutant A-site molecular switches may take the “off” state conformations in the absence of aminoglycoside. On the other hand, geneticin possessing strong affinities to both the wild type and the A1408G antibiotic-resistant mutant A sites [45] may have a potential to bind to and stabilize the “on” state of the lethal mutant switches in a similar way. Prior to crystallizations, 2 mM RNA solutions containing 100 mM sodium cacodylate (pH 7.0) were mixed with the same volume of 4 mM geneticin sulfate solution or distilled water. Crystallizations were performed by the hanging- and sitting-drop vapor diffusion methods at 293 K. Crystallization droplets were prepared by mixing 1  $\mu$ L of RNA solutions and 1  $\mu$ L of crystallization solutions containing 50 mM sodium cacodylate (pH 7.0), 1–10 mM spermine tetrahydrochloride, 10–300 mM monovalent or divalent cation chloride, 1%–10% (*v/v*) 2-methyl-2,4-pentanediol or polyethylene glycol 3350, and were equilibrated against 250  $\mu$ L of reservoir solution containing 40% (*v/v*) 2-methyl-2,4-pentanediol or polyethylene glycol 3350. For the A1408C lethal mutant, rhomboid-shaped crystals and polycrystals were obtained in conditions with and without geneticin (crystal codes: A1408C-Br/geneticin, A1408C-Br), respectively (Table S1). A polycrystal of A1408C-Br was crashed with an ultrafine needle to obtain small pieces of single crystals. For the A1408U lethal mutant, cubic- and rod-shaped single crystals were obtained in conditions with and without geneticin (crystal codes: A1408U/geneticin, A1408U), respectively (Table S2). The A1408C-Br/geneticin, A1408C-Br and A1408U/geneticin crystals obtained in conditions containing 2-methyl-2,4-pentanediol were picked up with CryoLoops (Hampton Research, Aliso Viejo, CA, USA) and directly flash-cooled in liquid nitrogen before X-ray experiments. The A1408U crystal obtained in a condition containing polyethylene glycol 3350 was picked up with CryoLoop, transferred to a droplet of 40% 2-methyl-2,4-pentanediol (cryoprotectant), and then flash-cooled in liquid nitrogen.

### 3.2. Data Collections, Structure Determinations and Refinements

X-ray data of the four crystals were collected at 100 K with synchrotron radiation at the BL-5A and BL-17A beamlines of the Photon Factory (Tsukuba, Japan). For the phase determination with the multiple anomalous diffraction (MAD) method, the X-ray datasets of the A1408C-Br/geneticin and A1408C-Br crystals were taken with four different wavelengths. The datasets were processed and scaled with the program Crystalclear (Rigaku Americas, The Woodlands, TX, USA). The intensity data were further converted to structure-factor amplitudes using the program TRUNCATE from the CCP4 suite [55]. The statistics of data collections are summarized in Table S3.

Initial phases of the A1408C-Br/geneticin and A1408C-Br crystals were estimated by the MAD method using the program AutoSol from the Phenix suite [56–58] with figure-of-merit of 0.41 and 0.83, respectively. The molecular structures of A1408C-Br/geneticin and A1408C-Br were constructed with the program COOT [59,60]. Initial phases of the A1408U/geneticin and A1408U-Br crystals were determined by the molecular replacement method with the program AutoMR from the Phenix suite [56,61] using an originally constructed model of the A-form RNA duplex as a probe, and then construction of their molecular structures were completed by using the program COOT.

The atomic parameters of each structure were refined with the program CNS [62,63] through a combination of simulated-annealing, crystallographic conjugate gradient minimization refinements and B-factor refinements. The statistics of structure refinements are summarized in Table S1. Molecular drawings were made using the program PyMOL [64]. The atomic coordinates and experimental data of the A1408C-Br/geneticin, A1408C-Br, A1408U/geneticin and A1408U crystals have been deposited in the Protein Data Bank (PDB) with the ID codes 4P3S, 4P3T, 4P43 and 4P3U, respectively.

**Supplementary Materials:** The following are available online, Supplementary Materials containing Tables S1–S3 and Figures S1–S5.

**Author Contributions:** Investigation, M.K.; Writing—review and editing and Supervision, J.K. All authors have read and agreed to the published version of the manuscript.

**Funding:** This work was supported by a Grant-in-Aid for Scientific Research (C) (No. 17K08248) from the Ministry of Education, Culture, Sports, Science and Technology, Japan (MEXT).

**Acknowledgments:** We thank the Photon Factory for provision of synchrotron radiation facilities (No. 2010G585, 2012G519, 2014G532, 2016G553 and 2018G565) and acknowledge the staff of the BL-5A and BL-17A beamlines.

**Conflicts of Interest:** The authors declare no conflict of interest.

### References

1. Ogle, J.M.; Carter, A.P.; Ramakrishnan, V. Insights into the decoding mechanism from recent ribosome structure. *Trends Biochem. Sci.* **2003**, *28*, 259–266. [[CrossRef](#)]
2. Ogle, J.M.; Carter, A.P.; Ramakrishnan, V. Structural insights into translation fidelity. *Annu. Rev. Biochem.* **2005**, *74*, 129–177. [[CrossRef](#)] [[PubMed](#)]
3. Noller, H.F. Biochemical characterization of the ribosomal decoding site. *Biochimie* **2006**, *88*, 935–941. [[CrossRef](#)] [[PubMed](#)]
4. Schmeing, T.M.; Ramakrishnan, V. What recent ribosome structures have revealed about the mechanism of translation. *Nature* **2009**, *461*, 1234–1242. [[CrossRef](#)] [[PubMed](#)]
5. Wimberly, B.T.; Brodersen, D.E.; Clemons, W.M., Jr.; Morgan-Warren, R.J.; Carter, A.P.; Vonnrhein, C.; Hartsch, T.; Ramakrishnan, V. Structure of the 30S ribosomal subunit. *Nature* **2000**, *407*, 327–339. [[CrossRef](#)]
6. Carter, A.P.; Clemons, W.M.; Brodersen, D.E.; Morgan-Warren, R.J.; Wimberly, B.T.; Ramakrishnan, V. Functional insights from the structure of the 30S ribosomal subunit and its interactions with antibiotics. *Nature* **2000**, *407*, 340–348. [[CrossRef](#)]
7. Ogle, J.M.; Brodersen, D.E.; Clemons, W.M., Jr.; Tarry, M.J.; Carter, A.P.; Ramakrishnan, V. Recognition of cognate transfer RNA by the 30S ribosomal subunit. *Science* **2001**, *292*, 897–902. [[CrossRef](#)]
8. Ogle, J.M.; Murphy, F.V.; Tarry, M.J.; Ramakrishnan, V. Selection of tRNA by the ribosome requires a transition from an open to a closed form. *Cell* **2002**, *111*, 721–732. [[CrossRef](#)]

9. Murphy, F.V., 4th; Ramakrishnan, V.; Malkiewicz, A.; Agris, P.F. The role of modifications in codon discrimination by tRNA(Lys)UUU. *Nat. Struct. Mol. Biol.* **2004**, *11*, 1186–1191. [[CrossRef](#)]
10. Murphy, F.V., 4th; Ramakrishnan, V. Structure of a purine-purine wobble base pair in the decoding center of the ribosome. *Nat. Struct. Mol. Biol.* **2004**, *11*, 1251–1252. [[CrossRef](#)]
11. Schuwirth, B.S.; Borovinskaya, M.A.; Hau, C.W.; Zhang, W.; Vila-Sanjurjo, A.; Holton, J.M.; Cate, J.H. Structures of the bacterial ribosome at 3.5 Å resolution. *Science* **2005**, *310*, 827–834. [[CrossRef](#)] [[PubMed](#)]
12. Selmer, M.; Dunham, C.M.; Murphy, F.V., 4th; Weixlbaumer, A.; Petry, S.; Kelley, A.C.; Weir, J.R.; Ramakrishnan, V. Structure of the 70S ribosome complexed with mRNA and tRNA. *Science* **2006**, *313*, 1935–1942. [[CrossRef](#)] [[PubMed](#)]
13. Dunham, C.M.; Selmer, M.; Phelps, S.S.; Kelley, A.C.; Suzuki, T.; Joseph, S.; Ramakrishnan, V. Structures of tRNAs with an expanded anticodon loop in the decoding center of the 30S ribosomal subunit. *RNA* **2007**, *13*, 817–823. [[CrossRef](#)] [[PubMed](#)]
14. Weixlbaumer, A.; Murphy, F.V., 4th; Dziergowska, A.; Malkiewicz, A.; Vendeix, F.A.; Agris, P.F.; Ramakrishnan, V. Mechanism for expanding the decoding capacity of transfer RNAs by modification of uridines. *Nat. Struct. Mol. Biol.* **2007**, *14*, 498–502. [[CrossRef](#)]
15. Kurata, S.; Weixlbaumer, A.; Ohtsuki, T.; Shimazaki, T.; Wada, T.; Kirino, Y.; Takai, K.; Watanabe, K.; Ramakrishnan, V.; Suzuki, T. Modified uridines with C5-methylene substituents at the first position of the tRNA anticodon stabilize U.G wobble pairing during decoding. *J. Biol. Chem.* **2008**, *283*, 18801–18811. [[CrossRef](#)]
16. Schmeing, T.M.; Voorhees, R.M.; Kelley, A.C.; Gao, Y.G.; Murphy, F.V., 4th; Weir, J.R.; Ramakrishnan, V. The crystal structure of the ribosome bound to EF-Tu and aminoacyl-tRNA. *Science* **2009**, *326*, 688–694. [[CrossRef](#)]
17. Schmeing, T.M.; Voorhees, R.M.; Kelley, A.C.; Ramakrishnan, V. How mutations in tRNA distant from the anticodon affect the fidelity of decoding. *Nat. Struct. Mol. Biol.* **2011**, *18*, 432–436. [[CrossRef](#)]
18. Neubauer, C.; Gillet, R.; Kelley, A.C.; Ramakrishnan, V. Decoding in the absence of a codon by tmRNA and SmpB in the ribosome. *Science* **2012**, *335*, 1366–1369. [[CrossRef](#)]
19. Demeshkina, N.; Jenner, L.; Westhof, E.; Yusupov, M.; Yusupova, G. A new understanding of the decoding principle on the ribosome. *Nature* **2012**, *484*, 256–259. [[CrossRef](#)]
20. Voorhees, R.M.; Mandal, D.; Neubauer, C.; Köhler, C.; RajBhandary, U.L.; Ramakrishnan, V. The structural basis for specific decoding of AUA by isoleucine tRNA on the ribosome. *Nat. Struct. Mol. Biol.* **2013**, *20*, 641–643. [[CrossRef](#)]
21. Fernández, I.S.; Ng, C.L.; Kelley, A.C.; Wu, G.; Yu, Y.T.; Ramakrishnan, V. Unusual base pairing during the decoding of a stop codon by the ribosome. *Nature* **2013**, *500*, 107–110. [[CrossRef](#)] [[PubMed](#)]
22. Demeshkina, N.; Jenner, L.; Westhof, E.; Yusupov, M.; Yusupova, G. New structural insights into the decoding mechanism: Translation infidelity via a G-U pair with Watson-Crick geometry. *FEBS Lett.* **2013**, *587*, 1848–1857. [[CrossRef](#)] [[PubMed](#)]
23. Vicens, Q.; Westhof, E. Crystal structure of paromomycin docked into the eubacterial ribosomal decoding A site. *Structure* **2001**, *9*, 647–658. [[CrossRef](#)]
24. Shandrick, S.; Zhao, Q.; Han, Q.; Ayida, B.K.; Takahashi, M.; Winters, G.C.; Simonsen, K.B.; Vourloumis, D.; Hermann, T. Monitoring molecular recognition of the ribosomal decoding site. *Angew. Chem. Int. Ed.* **2004**, *43*, 3177–3182. [[CrossRef](#)]
25. Kondo, J.; Urzhumtsev, A.; Westhof, E. Two conformational states in the crystal structure of the Homo sapiens cytoplasmic ribosomal decoding A site. *Nucleic Acids Res.* **2006**, *34*, 676–685. [[CrossRef](#)]
26. Kondo, J.; François, B.; Urzhumtsev, A.; Westhof, E. Crystal structure of the Homo sapiens cytoplasmic ribosomal decoding site complexed with apramycin. *Angew. Chem. Int. Ed. Engl.* **2006**, *45*, 3310–3314. [[CrossRef](#)]
27. Kondo, J.; Westhof, E. Structural comparisons between prokaryotic and eukaryotic ribosomal decoding A sites free and complexed with aminoglycosides. In *Aminoglycoside Antibiotics, from Chemical Biology to Drug Discovery*; Arya, D.P., Ed.; Wiley-Interscience: Hoboken, NJ, USA, 2007; pp. 209–223.
28. Kondo, J.; Westhof, E. The bacterial and mitochondrial ribosomal A-site molecular switches possess different conformational substates. *Nucleic Acids Res.* **2008**, *36*, 2654–2666. [[CrossRef](#)]
29. Kondo, J. A structural basis for the antibiotic resistance conferred by an A1408G mutation in 16S rRNA and for the antiprotozoal activity of aminoglycosides. *Angew. Chem. Int. Ed. Engl.* **2012**, *51*, 465–468. [[CrossRef](#)]

30. Kanazawa, H.; Baba, F.; Koganei, M.; Kondo, J. A structural basis of the antibiotic resistance conferred by an N1-methylation of A1408 in 16S rRNA. *Nucleic Acids Res.* **2017**, *45*, 12529–12535. [[CrossRef](#)]
31. Cannone, J.J.; Subramanian, S.; Schnare, M.N.; Collett, J.R.; D'Souza, L.M.; Du, Y.; Feng, B.; Lin, N.; Madabusi, L.V.; Müller, K.M.; et al. The comparative RNA web (CRW) site: An online database of comparative sequence and structure information for ribosomal, intron, and other RNAs. *BMC Bioinform.* **2002**, *3*, 2.
32. Prammananan, T.; Sander, P.; Brown, B.A.; Frischkorn, K.; Onyi, G.O.; Zhang, Y.; Böttger, E.C.; Wallace, R.J., Jr. A single 16S ribosomal RNA substitution is responsible for resistance to amikacin and other 2-deoxystreptomycin aminoglycosides in *Mycobacterium abscessus* and *Mycobacterium chelonae*. *J. Infect. Dis.* **1998**, *177*, 1573–1581. [[CrossRef](#)]
33. Sander, P.; Prammananan, T.; Böttger, E.C. Introducing mutations into a chromosomal rRNA gene using a genetically modified eubacterial host with a single rRNA operon. *Mol. Microbiol.* **1996**, *22*, 841–848. [[CrossRef](#)]
34. Suzuki, Y.; Katsukawa, C.; Tamaru, A.; Abe, C.; Makino, M.; Mizuguchi, Y.; Taniguchi, H. Detection of kanamycin-resistant *Mycobacterium tuberculosis* by identifying mutations in the 16S rRNA gene. *J. Clin. Microbiol.* **1998**, *36*, 1220–1225. [[PubMed](#)]
35. Alangaden, G.J.; Kreiswirth, B.N.; Aouad, A.; Khetarpal, M.; Igno, F.R.; Moghazeh, S.L.; Manavathu, E.K.; Lerner, S.A. Mechanism of resistance to amikacin and kanamycin in *Mycobacterium tuberculosis*. *Antimicrob. Agents Chemother.* **1998**, *42*, 1295–1297. [[CrossRef](#)] [[PubMed](#)]
36. Krüüner, A.; Jureen, P.; Levina, K.; Ghebremichael, S.; Hoffner, S. Discordant resistance to kanamycin and amikacin in drug-resistant *Mycobacterium tuberculosis*. *Antimicrob. Agents Chemother.* **2003**, *47*, 2971–2973. [[CrossRef](#)] [[PubMed](#)]
37. Maus, C.E.; Plikaytis, B.B.; Shinnick, T.M. Molecular analysis of cross-resistance to capreomycin, kanamycin, amikacin, and viomycin in *Mycobacterium tuberculosis*. *Antimicrob. Agents Chemother.* **2005**, *49*, 3192–3197. [[CrossRef](#)]
38. Feuerriegel, S.; Cox, H.S.; Zarkua, N.; Karimovich, H.A.; Braker, K.; Rüscher-Gerdes, S.; Niemann, S. Sequence analyses of just four genes to detect extensively drug-resistant *Mycobacterium tuberculosis* strains in multidrug-resistant tuberculosis patients undergoing treatment. *Antimicrob. Agents Chemother.* **2009**, *53*, 3353–3356. [[CrossRef](#)]
39. Jugheli, L.; Bzekalava, N.; de Rijk, P.; Fissette, K.; Portaels, F.; Rigouts, L. High level of cross-resistance between kanamycin, amikacin, and capreomycin among *Mycobacterium tuberculosis* isolates from Georgia and a close relation with mutations in the RRS gene. *Antimicrob. Agents Chemother.* **2009**, *53*, 5064–5068. [[CrossRef](#)]
40. Kogure, T.; Shimada, R.; Ishikawa, J.; Yazawa, K.; Brown, J.M.; Mikami, Y.; Gono, T. Homozygous triplicate mutations in three 16S rRNA genes responsible for high-level aminoglycoside resistance in *Nocardia farcinica* clinical isolates from a Canada-wide bovine mastitis epizootic. *Antimicrob. Agents Chemother.* **2010**, *54*, 2385–2390. [[CrossRef](#)]
41. Biswas, S.; Raoult, D.; Rolain, J.M. Molecular mechanism of gentamicin resistance in *Bartonella henselae*. *Clin. Microbiol. Infect.* **2009**, *15*, 98–99. [[CrossRef](#)]
42. Recht, M.I.; Douthwaite, S.; Puglisi, J.D. Basis for prokaryotic specificity of action of aminoglycoside antibiotics. *EMBO J.* **1999**, *18*, 3133–3138. [[CrossRef](#)] [[PubMed](#)]
43. Pfister, P.; Hobbie, S.; Vicens, Q.; Böttger, E.C.; Westhof, E. The molecular basis for A-site mutations conferring aminoglycoside resistance: Relationship between ribosomal susceptibility and X-ray crystal structures. *ChemBioChem* **2003**, *4*, 1078–1088. [[CrossRef](#)] [[PubMed](#)]
44. Gregory, S.T.; Carr, J.F.; Rodriguez-Correa, D.; Dahlberg, A.E. Mutational analysis of 16S and 23S rRNA genes of *Thermus thermophilus*. *J. Bacteriol.* **2005**, *187*, 4804–4812. [[CrossRef](#)] [[PubMed](#)]
45. Hobbie, S.N.; Pfister, P.; Brüll, C.; Westhof, E.; Böttger, E.C. Analysis of the contribution of individual substituents in 4,6-aminoglycoside-ribosome interaction. *Antimicrob. Agents Chemother.* **2005**, *49*, 5112–5118. [[CrossRef](#)] [[PubMed](#)]
46. Hobbie, S.N.; Pfister, P.; Bruell, C.; Sander, P.; François, B.; Westhof, E.; Böttger, E.C. Binding of neomycin-class aminoglycoside antibiotics to mutant ribosomes with alterations in the A site of 16S rRNA. *Antimicrob. Agents Chemother.* **2006**, *50*, 1489–1496. [[CrossRef](#)] [[PubMed](#)]

47. Hobbie, S.N.; Bruell, C.; Kalapala, S.; Akshay, S.; Schmidt, S.; Pfister, P.; Böttger, E.C. A genetic model to investigate drug-target interactions at the ribosomal decoding site. *Biochimie* **2006**, *88*, 1033–1043. [[CrossRef](#)]
48. Andersson, D.I. The biological cost of mutational antibiotic resistance: Any practical conclusions? *Curr. Opin. Microbiol.* **2006**, *9*, 461–465. [[CrossRef](#)]
49. Sander, P.; Springer, B.; Prammananan, T.; Sturmfels, A.; Kappler, M.; Pletschette, M.; Böttger, E.C. Fitness cost of chromosomal drug resistance-conferring mutations. *Antimicrob. Agents Chemother.* **2002**, *46*, 1204–1211. [[CrossRef](#)]
50. Shcherbakov, D.; Akbergenov, R.; Matt, T.; Sander, P.; Andersson, D.I.; Böttger, E.C. Directed mutagenesis of *Mycobacterium smegmatis* 16S rRNA to reconstruct the in-vivo evolution of aminoglycoside resistance in *Mycobacterium tuberculosis*. *Mol. Microbiol.* **2010**, *77*, 830–840. [[CrossRef](#)]
51. Taliaferro, D.L.; Farabaugh, P.J. Testing constraints on rRNA bases that make nonsequence-specific contacts with the codon-anticodon complex in the ribosomal A site. *RNA* **2007**, *13*, 1279–1286. [[CrossRef](#)]
52. Leontis, N.B.; Stombaugh, J.; Westhof, E. The non-Watson-Crick base pairs and their associated isostericity matrices. *Nucleic Acids Res.* **2002**, *30*, 3497–3531. [[CrossRef](#)] [[PubMed](#)]
53. Auffinger, P.; Hashem, Y. SwS: A solvation web service for nucleic acids. *Bioinformatics* **2007**, *23*, 1035–1037. [[CrossRef](#)] [[PubMed](#)]
54. Olson, W.K.; Bansal, M.; Burley, S.K.; Dickerson, R.E.; Gerstein, M.; Harvey, S.C.; Heinemann, U.; Lu, X.J.; Neidle, S.; Shakked, Z.; et al. A standard reference frame for the description of nucleic acid base-pair geometry. *J. Mol. Biol.* **2001**, *313*, 229–237. [[CrossRef](#)] [[PubMed](#)]
55. Collaborative Computational Project, Number 4. The CCP4 suite: Programs for protein crystallography. *Acta Crystallogr. D Biol. Crystallogr.* **1994**, *50*, 760–763. [[CrossRef](#)]
56. Adams, P.D.; Afonine, P.V.; Bunkóczi, G.; Chen, V.B.; Davis, I.W.; Echols, N.; Headd, J.J.; Hung, L.W.; Kapral, G.J.; Grosse-Kunstleve, R.W.; et al. PHENIX: A comprehensive Python-based system for macromolecular structure solution. *Acta Crystallogr. D Biol. Crystallogr.* **2010**, *66*, 213–221. [[CrossRef](#)]
57. Grosse-Kunstleve, R.W.; Adams, P.D. On symmetries of substructures. *Acta Crystallogr. D Biol. Crystallogr.* **2003**, *59*, 1974–1977. [[CrossRef](#)]
58. Terwilliger, T.C.; Adams, P.D.; Read, R.J.; McCoy, A.J.; Moriarty, N.W.; Grosse-Kunstleve, R.W.; Afonine, P.V.; Zwart, P.H.; Hung, L.W. Decision-making in structure solution using Bayesian estimates of map quality: The PHENIX AutoSol wizard. *Acta Crystallogr. D Biol. Crystallogr.* **2009**, *65*, 582–601. [[CrossRef](#)]
59. Emsley, P.; Cowtan, K. Coot: Model-building tools for molecular graphics. *Acta Crystallogr. D Biol. Crystallogr.* **2004**, *60*, 2126–2132. [[CrossRef](#)]
60. Emsley, P.; Lohkamp, B.; Scott, W.G.; Cowtan, K. Features and development of Coot. *Acta Crystallogr. D Biol. Crystallogr.* **2010**, *66*, 486–501. [[CrossRef](#)]
61. McCoy, A.J.; Grosse-Kunstleve, R.W.; Adams, P.D.; Winn, M.D.; Storoni, L.C.; Read, R.J. Phaser crystallographic software. *J. Appl. Crystallogr.* **2007**, *40*, 658–674. [[CrossRef](#)]
62. Brünger, A.T.; Adams, P.D.; Clore, G.M.; DeLano, W.L.; Gros, P.; Grosse-Kunstleve, R.W.; Jiang, J.S.; Kuszewski, J.; Nilges, M.; Pannu, N.S.; et al. Crystallography & NMR system: A new software suite for macromolecular structure determination. *Acta Crystallogr. D Biol. Crystallogr.* **1998**, *54*, 905–921. [[PubMed](#)]
63. Brünger, A.T. Free R value: A novel statistical quantity for assessing the accuracy of crystal structures. *Nature* **1992**, *355*, 472–475. [[CrossRef](#)] [[PubMed](#)]
64. DeLano, W.L. *The PyMOL Molecular Graphics System*; DeLano Scientific LLC: Palo Alto, CA, USA, 2008.

**Sample Availability:** Samples of the compounds are available from the authors.



© 2019 by the authors. Licensee MDPI, Basel, Switzerland. This article is an open access article distributed under the terms and conditions of the Creative Commons Attribution (CC BY) license (<http://creativecommons.org/licenses/by/4.0/>).